Technical University of Denmark

DTU

Ultralow power all-optical switch

Nguyen, H.; Grange, T.; Reznychenko, B.; Yeo, I.; De Assis, P.; Tumanov, D.; Fratini, F.; Malik, N.; Dupuy, E.; Gregersen, Niels; Auffèves, A.; Gérard, J.; Claudon, J.; Poizat, J.

[Link back to DTU Orbit](#)

DTU Library
Technical Information Center of Denmark

Ultralow power all-optical switch

H.A. Nguyen[1,2], T. Grange[1,2], B. Reznychenko[1,2], I. Yeo[1,2,3], P.-L. de Assis [4], D. Tumanov[1,2], F. Fratini[1,2], N.S. Malik[1,3], E. Dupuy[1,3], N. Gregersen[5], A. Auffèves[1,2], J.-M. Gérard[1,3], J. Claudon[1,3], and J.-Ph. Poizat[1,2,*]

[1] *Univ. Grenoble Alpes, 38000 Grenoble, France*
[2] *CNRS, Inst. NEEL, "Nanophysique et semiconducteurs" group, 38000 Grenoble France*
[3] *CEA, INAC-PHELIQS, "Nanophysique et semiconducteurs" group, 38000 Grenoble, France,*
[4] *Gleb Wataghin Institute of Physics, University of Campinas - UNICAMP, 13083-859, Campinas, São Paulo, Brazil*
[5] *Department of Photonics Engineering, DTU Fotonik, Kongens Lyngby, Denmark*
* *Corresponding author : jean-philippe.poizat@neel.cnrs.fr*
(Dated: May 12, 2017)

Optical logic down to the single photon level holds the promise of data processing with a better energy efficiency than electronic devices [1]. In addition, preservation of quantum coherence in such logical components could lead to optical quantum logical gates [2–4]. Optical logic requires optical non-linearities to enable photon-photon interactions. Non-linearities usually appear for large intensities, but discrete transitions allow for giant non-linearities operating at the single photon level [5], as demonstrated for a single optical mode with cold atomic gases [6, 7], or single two-level systems coupled to light via a tailored photonic environment [8–13]. However optical logic requires two-mode non-linearities [14, 15]. Here we take advantage of the large coupling efficiency and the broadband operation of a photonic wire containing a semiconductor quantum dot (QD) [16] to implement an all-optical logical component, wherein as few as 10 photons per QD lifetime in one mode control the reflectivity of another, spectrally distinct, mode.

Whether classical or quantum, optical communication has proven to be the best choice for long distance information distribution. All-optical data processing has therefore raised much interest in recent years, as it would avoid energy and coherence consuming optics-to-electronics conversion steps. Two-ports operation is a necessary requirement for the implementation of any non-trivial optical data processing. This involves a non-linear interaction between two distinct optical modes. Such a functionality operating at the single photon level can be achieved with a giant cross non-linearity obtained via resonant interactions in an atomic-like system featuring discrete energy levels [5].

Efficient coupling of a single light emitter to a propagating electromagnetic field is a key requirement to produce and manipulate a quantum state of light. This is achieved by engineering what has been coined a "one-dimensional atom" [17], in which a light emitter is predominantly coupled to a single propagating spatial mode. This favored coupling with a traveling mode is obtained either in a resonant optical cavity [8, 13] or with non-resonant field confinement such as in single transverse mode waveguides [12, 14] or through the interaction with a tightly focused optical beam [10, 15]. This favored coupling is the key element to extract light efficiently from a single emitter to produce an efficient source of single photons [16, 18–21]. Reversely, it is also the necessary ingredient to have a traveling wave interact with a single two-level system for quantum state transfer or to reach single photon non-linearities. Cavity implementations of this reversed situation have been realized with trapped atoms [3, 4, 8], and semiconductor QDs [2, 9, 11, 13], while cavity-free experiments have been carried out with single molecules [10] as well as with QDs [12, 14]. Note that such "one-dimensional atoms" have also been demon-

strated with superconducting circuits (see [22] for example).

The single mode giant non-linearity is based on the saturation of a single two-level system [23]. In a perfectly one-dimensional situation, a resonant laser, well below saturation, is totally reflected by a single two-level system, while it is completely transmitted above saturation. An all-optical switch requires two modes and can be implemented with a three-level structure wherein few photons in one mode control the reflection/transmission of light in the other one [11, 15, 22, 24, 25].

In this letter, we realize an all-optical switch triggered by as few as 10 photons per emitter lifetime. We use the non-degenerate three level structure of the biexciton-exciton (XX-X) cascade in a semiconductor InAs QD embedded in a GaAs waveguide (see Fig. 1a and Methods). Both excitonic and biexcitonic transitions of a QD located at the center of this broadband waveguide emit light preferentially in the fundamental guided mode, that adiabatically expands as it propagates along the conical taper [16]. The photons of both transitions can then be efficiently collected by a microscope objective and feature a large overlap with Gaussian beams [26]. For the same reasons, focusing mode-matched Gaussian beams on the top facet of the photonic wire, leads to a large interaction cross-section with both QD transitions.

The experimental set-up is depicted in Fig. 1b. It is based on a standard micro-photoluminescence set-up at a temperature of T=6K with two continuous wave lasers that can be finely tuned around each transition of the three-level scheme. By performing standard photoluminescence (PL) measurements of an individual QD using non-resonant laser excitation, we are able to identify the neutral X and XX transition energies, separated by 0.6 meV around 1.36 eV. We have measured lifetimes of 1.4 ns
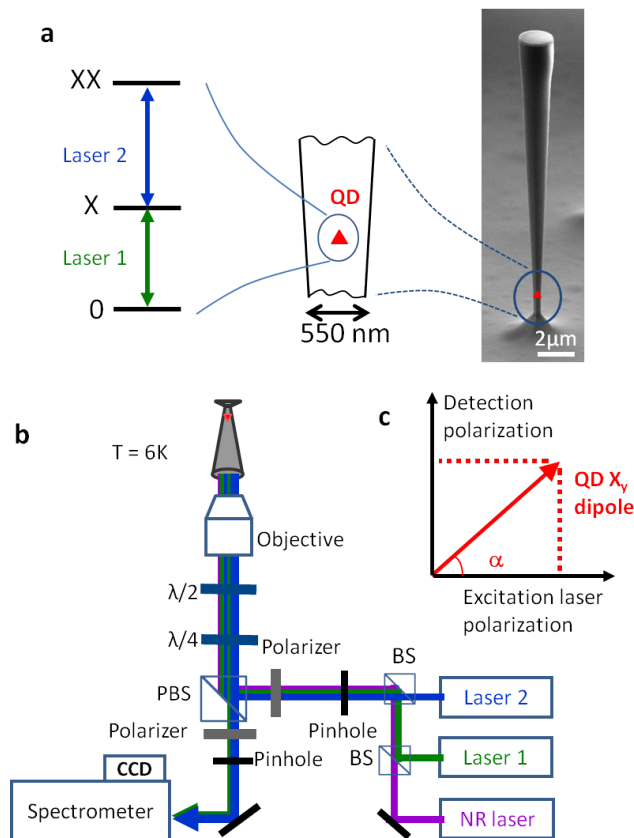
Figure 1. **Sample and set-up. a**, On the right, a scanning electron microscope image of the sample. In the center is shown the QD that is embedded at the bottom of the wire where the diameter provides an efficient coupling of the QD spontaneous emission to the fundamental guided mode. The empty QD, the excitonic (X) and biexcitonic (XX) states form a non-degenerate three-level ladder scheme as represented on the left. The two transitions are addressed by two different lasers. **b**, Experimental set-up. Two tunable continuous wave lasers excite the QD transitions. The lasers are spatially filtered with a pinhole located at the focal point of a lens. They are then focused on the sample with a microscope objective of 0.4 numerical aperture. A confocal detection with a pinhole selects only the light coming out of the photonic wire. An extra non-resonant (NR) laser is used for photoluminescence spectroscopy, and as a "quietening laser" during the experiments (see Methods). A polarizing beam splitter (PBS) is used for a cross-polarized detection scheme. **c**, The lasers are linearly polarized at an angle α with respect to the QD dipole of interest. The detection is performed along the polarization orthogonal to the laser polarization. Waveplates in front of the objective ensure a precise control of the lasers polarization [27].

(0.7 ns) for the excitonic (biexcitonic) level of the investigated QD. Owing to the non-perfect QD circular symmetry, the excitonic level features a fine structure splitting ($\approx 25\mu$eV, see SI) of the bright excitons (denoted X_x and X_y), which display orthogonal optical dipoles oriented along the cristallographic axis $x = [110]$ and $y = [1\text{-}10]$ of GaAs. In our experiments, we consider only one (X_y)

of the two dipoles. It exhibits a non-vanishing angle α with the lasers' linear polarization (see Fig. 1c). Thanks to a polarizing beam splitter, laser parasitic reflections are suppressed by a factor of 10^{-4}, while the light emitted by the QD dipole on the orthogonal polarization is detected by a charge coupled device (CCD) at the output of a grating spectrometer featuring a 12 μeV spectral resolution. Each laser is coupled with one of the two transitions of the three-level system, as described in Fig. 1. The switching effect is revealed by measuring the reflectivity of one of the lasers (probe laser) as a function of the intensity of the other one (control laser). We discuss below the two switch implementations corresponding to the control laser being tuned around the upper or lower transition of the three-level scheme.

We first consider the case in which the control (probe) laser is tuned on the lower (upper) transition (see Fig. 2). We will refer to this configuration as the "population switch", since the physics at work in this situation is the control of the X state population by the control laser. When the latter is off (Fig. 2a), both X and XX states are empty so that the probe laser sees a transparent medium and is totally transmitted. As the control laser intensity is increased towards saturation of the lower transition, the X state becomes populated so that the probe laser experiences a dipole-induced reflection (Fig. 2b).

This "population switch" mechanism is evidenced in Fig. 2c, which shows the probe laser reflectivity as a function of the control laser power. The switching threshold is only 1.6 nW (10 photons/lifetime), which is comparable to the best results obtained recently with a single molecule [15]. The probe reflectivity reaches a maximum for a control laser power as low as 16 nW (100 photons/lifetime). Increasing further the control laser power leads to an Autler-Townes splitting [28, 29] of the intermediate state, which brings the probe laser out of resonance and reduces its reflectivity.

This experimental behaviour is well fitted with our model over 4 orders of magnitude, for two different probe powers (see Methods and SI). The values of the reflectivity R and the switching power P_s are presently limited by imperfections of our system, and are fully accounted for by our model. The reflectivity scales as $R \sim \frac{\gamma}{\Gamma}\frac{\varepsilon^2}{\sin^2\alpha\cos^2\alpha}$, whereas the switching power scales as $P_s \sim \frac{\Gamma}{\gamma}\frac{\cos^2\alpha}{\varepsilon^2}$. In these expressions, γ is the lifetime limited linewidth, Γ the total linewidth, α the angle defined in Fig. 1c, and ε the fraction of input light coupled to the QD. The quantity ε is the product of the mode matching efficiency, the taper modal efficiency and the waveguide coupling efficiency β. From the global fitting of our experimental results, we extract $\varepsilon = 0.26 \pm 0.01$, which is in line with a Fourier modal method calculation [30] based on the sample geometry. In our experiment, the actual linewidth is $\Gamma = 10\gamma$. From the data fitting, we have estimated that this line broadening is distributed for one quarter into homogenous pure dephasing and for three quarters into inhomogeneous spectral diffusion.

With ideal parameters ($\varepsilon = 1$ and $\Gamma = \gamma$), losses are
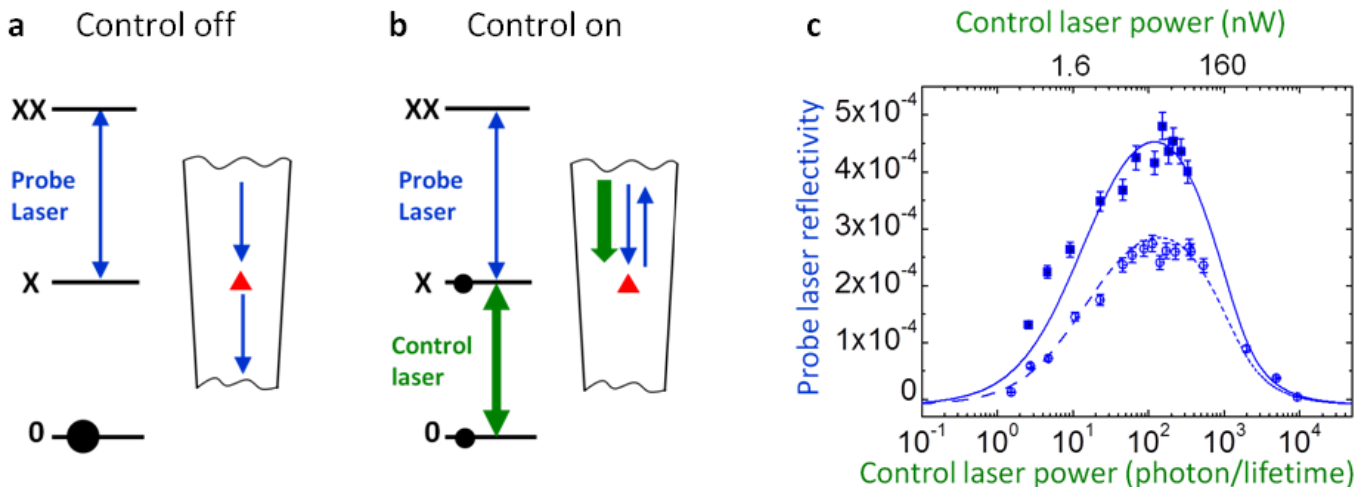
Figure 2. **Population switch.** The control (probe) laser is tuned around the lower (upper) transition. **a**, When the control laser is off, the probe laser sees an empty transition and is transmitted. **b**, When the control laser is on, the excitonic state is populated so that the probe laser is reflected. **c**, Probe reflectivity as a function of the control laser power, for a probe laser power of 0.5 nW (solid squares) and of 2.6 nW (empty circles). This corresponds to 0.1 and 0.5 of the saturation power. The solid and dashed lines are fits using our theoretical model with parameters that have also been used for the fitting of the data presented in Fig. 3

vanishing, so that less input light is required to saturate the QD. The contribution of the parasitic reflected light is therefore less important and the cross polarized detection scheme can be removed by aligning the laser polarizations to the exciton dipole direction and detect the reflected light along this polarization as well. This suppresses the projection terms depending on angle α in the reflectivity and switching power expressions. In the population switch case with ideal parameters, the switching power can be as low as $P_s = 0.1$ photons/lifetime but the maximum reflectivity can never exceed $R_{\max} = 0.1$, owing to the always partial population of the X state (cf. SI).

To overcome this fundamental limitation, we explore another switch mechanism in which the control (probe) laser is tuned on the upper (lower) transition (see Fig. 3). The physical effect here is the dressing of the upper transition when the control laser is well above saturation. In the absence of the control laser (Fig. 3a), the weak probe laser (below saturation) is reflected when on resonance with the lower transition [23]. When the control laser is turned on above saturation (Fig. 3b,c), the X state splits into two dressed states, as a result of the Autler-Townes effect [22, 28, 29]. The probe beam is then no longer resonant and its reflection switched off. In this "Autler-Townes" configuration, the switching threshold is found to be around 200 nW (cf. Fig. 3d). The Autler-Townes splitting effect is well evidenced in Fig. 3e-g) exhibiting the typical anticrossing of the probe laser reflectivity as a function of the two laser detunings. Using the same set of parameters for all the data presented in this work, our theoretical model is able to reproduce with a good accuracy our experimental results (Figs. 2,3). For completeness, data showing the influence of the two bright excitons are shown in the SI.

Interestingly, and contrary to the population switch configuration, the "Autler-Townes" configuration potentially shows perfect performances (i.e. $R_{\max} = 1$, $P_s = 1$ photons/lifetime) with ideal parameters ($\varepsilon = 1$ and $\Gamma = \gamma$) in the copolarized setting (cf. SI). Moreover, our theoretical model indicates that, in this case, the reflectivity is almost fully coherent which is a key asset in the perspective of the realization of quantum logical gates (cf. SI) [5].

Let us mention that these ideal parameters are not so far ahead. Values as high as $\varepsilon = 0.75$ have already been reported in slightly narrower waveguides and expected values for optimized designs are as high as $\varepsilon = 0.95$ [16]. Additionally, close to lifetime-limited linewidths (i.e. $\Gamma = \gamma$) have been obtained recently by applying a voltage bias across the QD [20, 31].

In conclusion, we have experimentally demonstrated an all-optical switch with a switching power of 10 photons per emitter lifetime. Such all-optical devices are relevant for energy efficient logical operations and paves the way for coherent operations enabling quantum logical gates. Furthermore, when integration is required, these results can be transferred to planar waveguide geometries such as photonic crystals [12], or silicon based photonic circuits [32, 33], and offer therefore interesting perspectives for on-chip photonic computation.
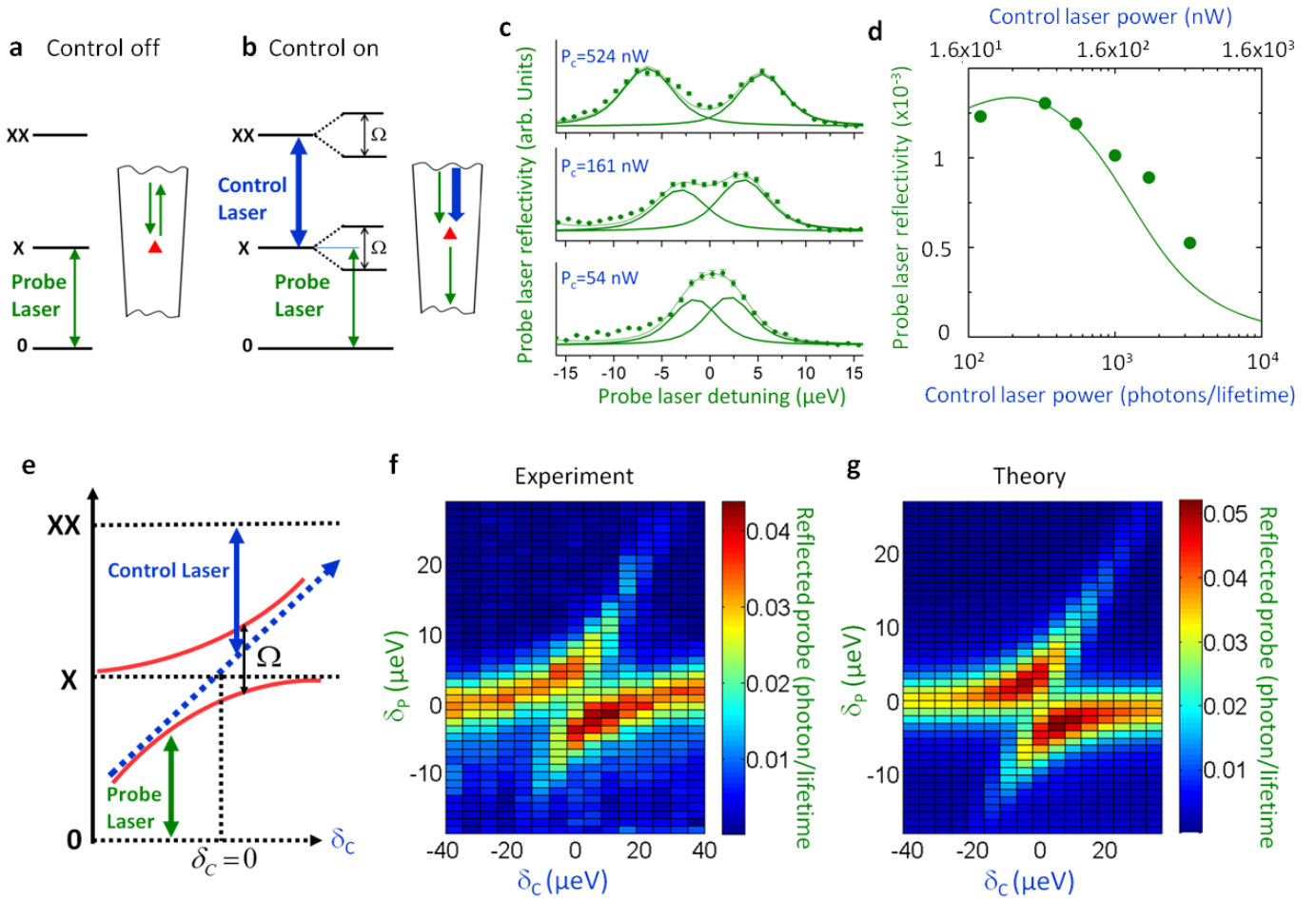
Figure 3. **Switch in the Autler-Townes configuration**. The control (probe) laser is tuned on the upper (lower) transition. **a**, when the control laser is off, the probe is reflected. **b**, when the control laser is on, it splits the X state, so that the probe is no longer on resonance, and therefore transmitted. **c**, Probe reflectivity as a function of its detuning for different control laser powers, and a zero control laser detuning. The solid line are fits using individual line profile with the line position as a free parameter. The thinner line is the sum of the individual lines. We have checked that the splitting scales as the square root of the control laser power (data not shown) **d**, Probe reflectivity as a function of the control laser power. The probe laser power is 1 nW. The solid line is the result given by our theoretical model. **e**, Position of the Autler-Townes doublet as the control laser is scanned across the upper transition. **f**, experimental (see Methods), and **g**, theoretical reflectivity of the probe laser as a function of probe and control laser detunings. The probe (control) laser power is 1 nW (274 nW). The theoretical fits are all made with the same set of parameters as in Fig.2c.

METHODS

A quantum dot in a photonic wire

The sample studied in this work is made of epitaxial GaAs and has the shape of an inverted cone lying on a pyramidal pedestal. The inverted cone is 17.2 μm high, the diameter at the waist is 0.5 μm and the top facet diameter is 1.9 μm. This "photonic trumpet" embeds a single layer of a few tens of self-assembled InAs QDs, located 0.8 μm above the waist (position determined by cathodoluminescence). To optimize the light extraction efficiency, the top facet is covered by an anti-reflection coating (115 nm thick Si_3N_4 layer). To suppress spurious surface effects, the wire sidewalls are passivated with a 20 nm thick Si_3N_4 layer. We define such structures with a top-down process, very similar to the one described in [16].

Importance of the non-resonant laser

The obtention of narrow resonant lines of the QD transitions requires the presence of a non-resonant laser ($\lambda = 825$nm, i.e. $E = 1.5$eV). The power of this laser is always kept around 0.1nW (i.e. 10^{-3} times the saturation power), so that its induced photoluminescence remains negligible compared to the resonant laser luminescence. The carriers generated in the wetting layer by this weak non-resonant laser have been shown to reduce

spectral diffusion and hence reduce the linewidth [34]. This is a standard technique in resonant excitation experiments with individual QDs. In our case the linewidth is reduced by a factor of 3, from 15μeV down to 5μeV.

Extraction of experimental parameters

The unknown parameters of the QD-waveguide system are the input-output coupling efficiency ε, the pure dephasing rate γ^* and the spectral diffusion factor w_{diff}. The factor ε is extracted very precisely from the Autler-Townes splitting results (see Fig. 3), wherein the control laser is well above saturation and dresses the upper transition for one of the fine structure split level ($|X_y\rangle$ for example), while the well below saturation probe laser probes the Autler-Townes splitting induced by the control laser. The Autler-Townes splitting is given by $\Omega = \sqrt{\delta_2^c + \Omega_c^2}$, where δ_c is the detuning between the control laser and the $|X_y\rangle - |XX\rangle$ transition, and Ω_c is the Rabi frequency of the control laser that directly interacts with the QDs inside the photonic wire. We have $\Omega_c^2 = 2\varepsilon\gamma I_c^{\mathrm{in}}$, where I_c^{in} is the control laser intensity (in photons per excitonic lifetime) at the input of the photonic wire [35]. By measuring Ω at zero-detuning ($\delta_c = 0$), and comparing with I_c^{in}, we find a coupling efficiency factor $\varepsilon = 0.26 \pm 0.01$.

The next unknown factors are the pure dephasing γ^* and the broadening induced by spectral diffusion w_{diff} (see SI). A total linewidth of 4μeV has been measured from the resonant laser scans (see Fig. 3c,f). The weight between the two broadening mechanisms is then determined by optimizing the fits with the experimental results. This leads us to take $\gamma^* = 1 \pm 0.5\mu$eV and $w_{\mathrm{diff}} = 3 \pm 0.5\mu$eV.

Observation of the Autler-Townes splitting

To experimentally evidence the Autler-Townes effect, the two lasers are respectively scanned across the frequencies of lower and upper transitions and the probe reflectivity is recorded (see Fig. 3f). At each step of the scan, the spectrum of the light reflected from the trumpet is recorded on a CCD camera with a typical integration time of 0.1s. The probe reflectivity is obtained by integrating the counts within a fixed spectral interval of more than 100μeV containing the probe laser scan interval (max 80μeV), and including therefore both fine structure split levels.

[1] Miller, D.A., Are optical transistors the logical next step? Nat. Photon. **4**, 3 (2010).

[2] Kim, H., Bose, R., Shen, T.C., Solomon, G.S. and Waks, E., A quantum logic gate between a solid-state quantum bit and a photon. Nat. Photon. **7**, 373 (2013).

[3] Reiserer, A., Kalb, N., Rempe, G., Ritter, S., A quantum gate between a flying optical photon and a single trapped atom, Nature **508**, 237 (2014).

[4] Tiecke, T.G., Thompson, J.D., de Leon, N.P., Liu, L.R., Vuletić, V., and Lukin, M.D., Nanophotonic quantum phase switch with a single atom, Nature **508**, 241 (2014).

[5] Chang, D.E., Vuletic, V. and Lukin, M.D., Quantum nonlinear optics photon by photon. Nature Photon. **8**, 685 (2014).

[6] Baur, S., Tiarks, D., Rempe, G., Dürr, S., Single-Photon Switch Based on Rydberg Blockade, Phys. Rev. Lett. **112**, 073901 (2014).

[7] Chen, W., Beck, K.M., Bücker, R., Gullans, M., Lukin, M.D., Tanji-Suzuki, H., Vuletić, V., All-Optical Switch and Transistor Gated by One Stored Photon Science **341**, 768 (2013).

[8] Birnbaum, K.M., et al, Photon blockade in an optical cavity with one trapped atom. Nature (London) **436**, 87 (2005).

[9] Fushman, I., et al. Controlled phase shifts with a single quantum dot. Science **320**, 769-772 (2008).

[10] Hwang, J., Pototschnig, M. , Lettow, R., Zumofen, G., Renn, A., Götzinger, S., and Sandoghdar, V., A single-molecule optical transistor, Nature (London) **460**, 76 (2009).

[11] Volz, T., Reinhard, A., Winger, M., Badolato, A., Hennessy, K.J., Hu, E.L., and Imamoğlu, A., Ultrafast all-optical switching by single photons, Nature Photon. **6**, 605 (2012).

[12] Javadi, A., et al, Single-photon non-linear optics with a quantum dot in a waveguide, Nat. Commun. **6**, 8655 (2015).

[13] Giesz, V., et al, Coherent manipulation of a solid-state artificial atom with few photons, Nat. Commun. **7**, 11986 (2016).

[14] Chang, D.E., Sørensen, A.S., Demler, E.A. and Lukin., M.D. A single-photon transistor using nanoscale surface plasmons, Nat. Phys. **3**, 807 (2007).

[15] Maser, A., Gmeiner, B., Utikal, T., Götzinger, S. and Sandoghdar, V., Few-photon coherent nonlinear optics with a single molecule, Nature Photon. **10**, 450 (2016).

[16] Munsch, M., Malik, N.S., Dupuy, E., Delga, A., Bleuse, J., Gérard, J.M. and Claudon, J., Dielectric GaAs Antenna Ensuring an Efficient Broadband Coupling between an InAs Quantum Dot and a Gaussian Optical Beam, Phys. Rev. Lett. **110**, 177402 (2013).

[17] Turchette, Q.A., Thomson, R.J., and Kimble, H.J., "One-dimensional atoms", Appl. Phys. B **60**, S1 (1995).

[18] Claudon, J., Bleuse, J., Malik, N.S., Bazin, M., Jaffrennou, P., Gregersen, N., Sauvan, C., Lalanne, P. and Gérard, J.M., A highly efficient single-photon source based on a quantum dot in a photonic nanowire, Nat. Photon. **4**, 174 (2010).

[19] Lee K.G., Chen, X.W., Eghlidi, H., Kukura P., Lettow, R., Renn, A., Sandoghdar, V., Götzinger, S., A planar dielectric antenna for directional single-photon emission and near-unity collection efficiency, Nat. Photon. **5**, 166 (2011).

[20] Somaschi, N., et al, Near-optimal single-photon sources in the solid state, Nat. Photon. **10**, 340 (2016).

[21] Ding, X., et al, On-Demand Single Photons with High Extraction Efficiency and Near-Unity Indistinguishability from a Resonantly Driven Quantum Dot in a Micropillar, Phys. Rev. Lett. **116**, 020401 (2016).

[22] Hoi, I.C., Wilson, C.M., Johansson, G., Palomaki, T., Peropadre, B., Delsing., P., Demonstration of a Single-Photon Router in the Microwave Regime, Phys. Rev. Lett. **107**, 073601 (2011).

[23] Auffèves-Garnier, A., Simon, C., Gérard, J.M., Poizat, J.P., Giant Optical Non-linearity induced by a Single Two-Level System interacting with a Cavity in the Purcell Regime, Phys. Rev. A **75**, 053823 (2007).

[24] Englund, D., Majumdar, A., Bajcsy, M., Faraon, A., Petroff, P. and Vučković, J., Ultrafast Photon-Photon Interaction in a Strongly Coupled Quantum Dot-Cavity System, Phys. Rev. Lett. **108**, 093604 (2012).

[25] Bose, R., Sridharan, D., Kim, H., Solomon, G.S., and Waks, E., Low-Photon-Number Optical Switching with a Single Quantum Dot Coupled to a Photonic Crystal Cavity, Phys. Rev. Lett. **108**, 227402 (2012).

[26] Stepanov, P., Delga, A., Gregersen, N., Peinke, E., Munsch, M., Teissier, J., Mørk, J., Richard, M., Bleuse, J., Gérard, J.M.,and Claudon, J., Highly directive and Gaussian far-field emission from giant photonic trumpets, Appl. Phys. Lett. **107**, 141106 (2015).

[27] Kuhlmann, A.V., Houel, J., Brunner, D., Ludwig, A., Reuter, D., Wieck, A.D., and Warburton, R.J., A dark-field microscope for background-free detection of resonance fluorescence from single semiconductor quantum dots operating in a set-and-forget mode, Rev. Sci. Instrum. **84**, 073905 (2013).

[28] Autler, S.H., Townes, C.H., Stark Effect in Rapidly Varying Fields, Phys. Rev. **100**, 703 (1955)

[29] Xu, X., Sun, B., Berman, P.R., Steel, D.G.,Bracker, A.S., Gammon, D., Sham, L.J., Coherent Optical Spectroscopy of a Strongly Driven Quantum Dot, Science, **317**, 929 (2007).

[30] Häyrynen, T., de Lasson, J.R., and Gregersen, N., Open-geometry Fourier modal method: Modeling nanophotonic structures in infinite domains, J. Opt. Soc. Am. A **33**, 1298 (2016).

[31] Kuhlmann, A.V., Prechtel, J.H., Houel, Ludwig, J.A., Reuter, D., Wieck, A.D. and Warburton, R.J., Transform-limited single photons from a single quantum dot, Nat. Commun. **6**, 8204 (2015).

[32] Politi, A., Cryan, M.J., Rarity, J.G., Yu, S., O'Brien, J.L., Silica-on-silicon waveguide quantum circuits, Science **320**, 646 (2008).

[33] Esmaeil Zadeh, I., et al, Deterministic Integration of Single Photon Sources in Silicon Based Photonic Circuits, Nano Lett. **16**, 2289 (2016).

[34] Majumdar, A., Kim, E.D., and Vučković, J., Effect of photogenerated carriers on the spectral diffusion of a quantum dot coupled to a photonic crystal cavity, Phys. Rev. B **84**, 195304 (2011).

[35] Valente, D., Portolan, S., Nogues, G., Poizat, J.P., Richard, M., Gérard, J.M., Santos, M.F. and Auffèves, A., Monitoring stimulated emission at the single-photon level in one-dimensional atoms, Phys. Rev. A **85**, 023811 (2012).

SUPPLEMENTARY INFORMATION

A. Theoretical model

a. Master equation for the electronic system. We consider the 4-level system formed by the electronic eigenstates $|0\rangle, |X_x\rangle, |X_y\rangle, |XX\rangle$. Under laser driving, the system Hamiltonian can be written as

$$H = H_0 + H_L, \qquad (1)$$

where H_0 represents the electronic part, and H_L the interaction with a coherent optical drive within the rotating-wave approximation (see e.g. [1])

$$H_0 = E_{X_x}|X_x\rangle\langle X_x| + E_{X_y}|X_y\rangle\langle X_y| + E_{XX}|XX\rangle\langle XX| \qquad (2)$$

$$H_L = \frac{\hbar\Omega_1}{2}e^{i\omega_1 t}|0\rangle\langle X_h| + \frac{\hbar\Omega_2}{2}e^{i\omega_2 t}|X_h\rangle\langle XX| + \text{h.c.}, \qquad (3)$$

where h (v) is the polarization along (perpendicular to) the lasers, and $|X_h\rangle = \cos\alpha|X_y\rangle + \sin\alpha|X_x\rangle$ the exciton mode along this polarization ($|X_v\rangle = \sin\alpha|X_y\rangle - \cos\alpha|X_x\rangle$). The quantities $\omega_{1,2}/2\pi$ are the laser frequencies, and $\Omega_{1,2}/2\pi$ the corresponding Rabi Frequencies. The Lindblad master equation for the density matrix ρ reads [2]

$$\frac{\partial\rho}{\partial t} = \frac{i}{\hbar}[\rho, H] + \mathcal{L}_{\text{decay}} + \mathcal{L}_{\text{dephasing}}, \qquad (4)$$

where $\mathcal{L}_{\text{decay}}$ describes the radiative decay processes and $\mathcal{L}_{\text{dephasing}}$ the pure dephasing processes. They read respectively

$$\mathcal{L}_{\text{decay}} = \gamma L_{|X_x\rangle\langle 0|}(\rho) + \gamma L_{|X_y\rangle\langle 0|}(\rho) \\ + \gamma L_{|XX\rangle\langle X_x|}(\rho) + \gamma L_{|XX\rangle\langle X_y|}(\rho) \qquad (5)$$

$$\mathcal{L}_{\text{dephasing}} = \frac{\gamma^*}{2} L_{|X_x\rangle\langle X_x| + |X_y\rangle\langle X_y| - |0\rangle\langle 0|}(\rho) \\ + \frac{\gamma^*}{2} L_{|XX\rangle\langle XX| - |X_x\rangle\langle X_x| - |X_y\rangle\langle X_y|}(\rho) \qquad (6) \\ + \frac{\gamma^*}{2} L_{|XX\rangle\langle XX| - |0\rangle\langle 0|}(\rho),$$

where $L_C(\rho)$ is the Lindblad superoperator for a collapse operator C:

$$L_C(\rho) = \left[C\rho C^\dagger - \frac{1}{2}\left(\rho C^\dagger C + C^\dagger C\rho\right)\right]. \qquad (7)$$

In the radiative decay term $\mathcal{L}_{\text{decay}}$, we have assumed that the four different possible exciton recombination processes occur at the same rate γ. In the pure dephasing term $\mathcal{L}_{\text{dephasing}}$, an additional decay of the coherence between the ground state, the excitonic states and the biexciton state is considered with a rate $\gamma^*/2$, corresponding to an additional spectral broadening of $\hbar\gamma^*$ for the full width at half maximum (FWHM) of these transitions.
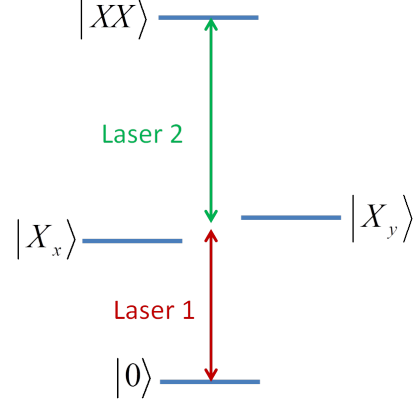

Figure 4. **Level scheme**. Levels $|X_x\rangle$ and $|X_y\rangle$ are the two fine structure split excitonic eigenstates. In practice they are separated by 25 μeV, and we can consider only one of them. Level $|XX\rangle$ corresponds to the biexciton. Laser 1 (2) is tuned around the lower (upper) transition.

b. Optical nonlinearities. The optical nonlinearities are calculated following previous studies of quantum electrodynamics in one-dimensional wave-guides [3, 4]. The total reflected intensity (in photons per unit time) for the transition 1 (2) is proportional to the exciton (biexciton) population:

$$I_{1,p}^{\text{R}} = \varepsilon\frac{\gamma}{2}n_{X_p}, \qquad (8)$$

$$I_{2,p}^{\text{R}} = \varepsilon\frac{\gamma}{2}n_{XX}, \qquad (9)$$

where $p = v$ or h is the polarization, $n_i = \rho_{ii}$ is the population of the level i, and ε is the product of the mode matching efficiency with the waveguide coupling efficiency β (see main text). The coherent part of these reflected intensities reads

$$I_{1,p}^{\text{Rcoh}} = \varepsilon\frac{\gamma}{2}|\langle 0|\rho|X_p\rangle|^2, \qquad (10)$$

$$I_{2,p}^{\text{Rcoh}} = \varepsilon\frac{\gamma}{2}|\langle X_p|\rho|XX\rangle|^2. \qquad (11)$$

In the polarization v (orthogonal to the excitation's one), the transmitted intensity is equal to the reflected one $I_v^{\text{T}} = I_v^{\text{R}}$ since the quantum dot (QD) luminescence is distributed symmetrically between the two directions without any interference with the incident beam. In contrast, for the polarization h (parallel to the excitation's one), an interference effect occurs between the incident field and the scattered field. The coherent and total (i.e. coherent + incoherent) transmitted electric fields are given respectively for the transitions 1 and 2 by

$$I_{1,h}^{\text{Tcoh}} = \varepsilon\left|\sqrt{\varepsilon I_1^{\text{in}}} + i\sqrt{\frac{\gamma}{2}}\langle 0|\rho|X_h\rangle\right|^2 \qquad (12)$$

$$I_{1,h}^{\mathrm{T}} = \varepsilon \left[I_1^{\mathrm{in}} + \frac{\gamma}{2} n_{\mathrm{X}_p} + \sqrt{2\gamma I_{\mathrm{in}}} \, \mathrm{Im}\left(\langle 0|\rho|\mathrm{X}_h\rangle\right) \right] \quad (13)$$

$$I_{2,h}^{\mathrm{Tcoh}} = \varepsilon \left| \sqrt{\varepsilon I_2^{\mathrm{in}}} + i\sqrt{\frac{\gamma}{2}} \langle \mathrm{X}_h|\rho|\mathrm{XX}\rangle \right|^2 \quad (14)$$

$$I_{2,h}^{\mathrm{T}} = \varepsilon \left[I_2^{\mathrm{in}} + \frac{\gamma}{2} n_{\mathrm{XX}} + \sqrt{2\gamma I_2^{\mathrm{in}}} \, \mathrm{Im}\left(\langle \mathrm{X}_h|\rho|\mathrm{XX}\rangle\right) \right] \quad (15)$$

c. Spectral diffusion In addition to pure dephasing, we consider spectral diffusion processes, i.e. fluctuation of the electronic transition energies over timescales which are long compared to the exciton lifetime $1/\gamma$. A fluctuating term δE_{X} in the exciton energy is added as:

$$E_{\mathrm{X}_i} = E_{\mathrm{X}_i}^0 + \delta E_{\mathrm{X}} \quad (16)$$

$$E_{\mathrm{XX}} = E_{\mathrm{XX}}^0 + 2\delta E_{\mathrm{X}} \quad (17)$$

where $i = x, y$, and $E_{\mathrm{X}_i}^0$ (E_{XX}^0) is the mean exciton (biexciton) energy. This fluctuation is assumed to verify a Gaussian distribution, with a probability density function:

$$\mathcal{P}(\delta E_{\mathrm{X}}) = \frac{1}{\sigma_{\mathrm{X}}\sqrt{2\pi}} \exp\left[-\frac{\delta E_{\mathrm{X}}^2}{2\sigma_{\mathrm{X}}^2} \right] \quad (18)$$

where σ_{X} is the standard deviation. The corresponding FWHM reads $w_{\mathrm{diff}} = 2\sqrt{2\ln(2)}\sigma_{\mathrm{X}}$. The total FWHM of the excitonic and biexcitonic transitions reads

$$\Gamma = \gamma + \gamma^* + w_{\mathrm{diff}} \quad (19)$$

For each realization of spectral diffusion, we calculate the density matrix $\rho(\delta E_{\mathrm{X}})$ under continuous-wave excitation by finding the steady-state of the above Lindblad equation (Eq. 4). The density matrix and the reflectivities are then averaged over the distribution $\mathcal{P}(\delta E_{\mathrm{X}})$.

d. Effective 3-level system. For Rabi frequencies and detunings which remains small compared to the fine structure splitting ($E_{\mathrm{X}_y} - E_{\mathrm{X}_x} = 27$ µeV), the system behaves as a 3-level system ($|0\rangle, |\mathrm{X}_y\rangle, |\mathrm{XX}\rangle$), i.e. the influence of the state $|\mathrm{X}_x\rangle$ is negligible. The light-matter interaction can be written

$$H_L^{\mathrm{eff}} = \frac{\hbar\Omega_1^{\mathrm{eff}}}{2} e^{i\omega_1 t}|0\rangle\langle \mathrm{X}_y| + \frac{\hbar\Omega_2^{\mathrm{eff}}}{2} e^{i\omega_2 t}|\mathrm{X}_y\rangle\langle \mathrm{XX}| + \mathrm{h.c.}, \quad (20)$$

with $\Omega_i^{\mathrm{eff}} = \Omega_i \sin\alpha$. In addition, a factor $\cos\alpha$ (or $\cos^2\alpha$) appears when expressing the coherences (or populations) of the horizontal exciton mode for cross-polarized reflections, such as $\langle 0|\rho|\mathrm{X}_h\rangle = \langle 0|\rho|\mathrm{X}_y\rangle \cos\alpha$ and $n_{\mathrm{X}_h} = n_{\mathrm{X}_y} \cos^2\alpha$.
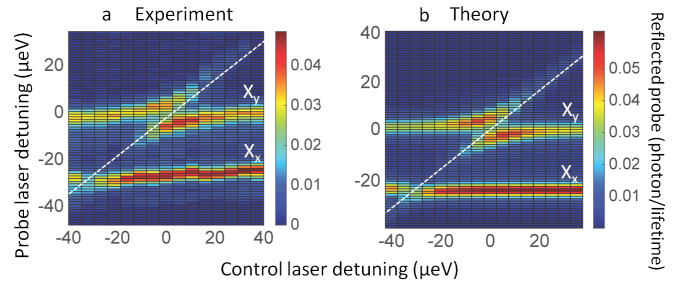

Figure 5. **Fine structure splitting.** Experimental (left) and theoretical (right) results following Autler-Townes splitting approach including both excitonic levels X_x and X_y split by 25 µeV. The probe reflected intensity is plotted as function of control and probe detunings. The control laser power is set at 274 nW. The probe laser scanning range is 80 µeV. The white dashed lines are guides to the eye corresponding to the positions of the control laser beam during the scan. The model uses the coupling efficiencies $\varepsilon_{in} = \varepsilon_{out} = 0.26$ and the total linewidth broadening 4 µeV, including 1 µeV pure dephasing and 3 µeV spectral diffusion, as for all the data presented in this work.

B. Experimental data including the fine structure splitting

In this section, we give a complete picture concerning the presence of the other excitonic dipole in the Autler-Townes splitting approach. To this end, we have carried out a broad scan of the probe beam covering both excitonic states X_x and X_y. Fig. 5 shows the experimental and theoretical results for a scan with a control laser power 274 nW. The Autler-Townes splitting is observed for both states. It should be mentioned that the splittings are different for each state, because, except for $\alpha = 45°$, the two orthogonally polarized excitonic dipoles are excited differently with respect to the resonant laser polarization. The Autler-Townes splittings at resonance for the two dipoles, Ω_x and Ω_y scale as $\Omega_y/\Omega_x = 1/\tan\alpha$, with α the angle between the polarizations of laser and X_y as defined in Fig. 1 of the main text. In our experiment, we have chosen $\alpha = 27°$ so that $\Omega_y/\Omega_x \approx 2$.

C. Switch performances in ideal conditions

In this section we compute the reflectivity with ideal parameters ($\varepsilon = \Gamma/\gamma = 1$). The total reflectivity is given by equations (8,9), whereas the coherent part is given by equations (10,11).

1. Population switch configuration

In this approach, the control (probe) beam is tuned on the lower (upper) transition (cf. Fig. 2 of the main text). The switching effect is based on a population effect, so that incoherent scattering is dominant even with
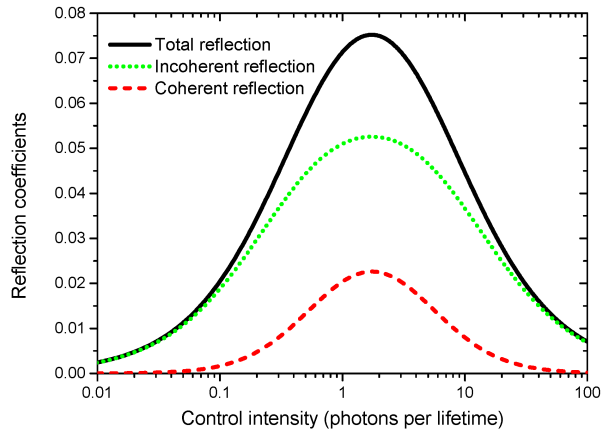
below, the Autler-Townes configuration offers very good performance, including coherence, for ideal parameters.

Figure 6. **Ideal probe reflectivity in the population switch case**. The computed reflectivity of a vanishingly weak probe laser (tuned on the upper transition) is plotted as a function of the control laser power (tuned on the lower transition) in a copolarized situation with ideal parameters ($\varepsilon = \Gamma/\gamma = 1$). The probe power is 10^{-3} photon/lifetime. It can be observed that the reflection is mainly incoherent.

ideal parameters (see Fig. 6). Additionally, owing to the never complete population of the X_y state, the maximum reflectivity never exceeds $R = 0.1$.

a. Cross-polarized. Here the detected light is linearly polarized orthogonally to the input laser, as in our experiment, to ensure a low level of parasitic backscattered laser light. The other fine-structure splitting level X_x, which is also populated via the XX state, also contributes to the probe reflectivity in an incoherent way, so that the total reflectivity is mainly incoherent. For $\alpha = 45^\circ$), its maximum value is $R = 0.03$ obtained for 1 photon/lifetime.

b. Co-polarized. In the case of low backscattered light from the trumpet top facet, we can in principle access the light reflected from the trumpet along the same polarization as the input laser. In this situation the relevant QD dipole is chosen along this polarization. Even in this case, the population switch configuration does not allow for unity reflectivity (see Fig.6), owing to the never complete population of the X_y state. Since half of the reflectivity is due to the other excitonic state (X_x state), only half of the reflected light is coherent.

2. Autler-Townes configuration

In the Autler-Townes approach, the control (probe) is tuned on the upper (lower) transition. As it is shown

a. Cross-polarized. For $\alpha = 45^\circ$, the maximum reflectivity is limited by the term $(1/2)\cos^2\alpha\sin^2\alpha =$
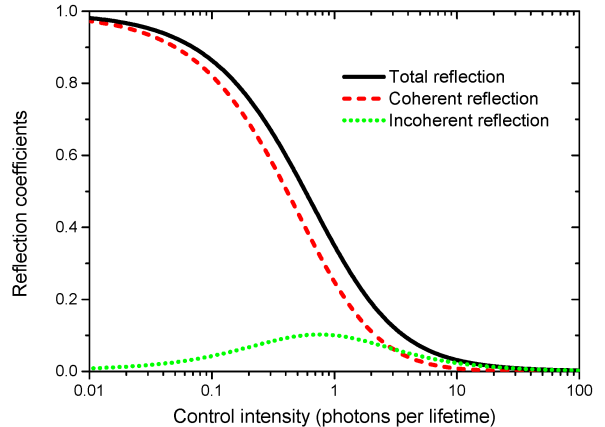

Figure 7. **Ideal probe reflectivity in the Autler-Townes configuration**. The computed reflectivity of a vanishingly weak probe laser (tuned on the lower transition) is plotted as a function of the control laser power (tuned on the upper transition) in a copolarized situation with ideal parameters ($\varepsilon = \Gamma/\gamma = 1$). The probe power is 10^{-3} photon/lifetime. The reflectivity is mainly coherent and reaches unity at low control laser power.

0.125 where the $1/2$ factor comes from the fact that, owing to the orthogonal polarization, the reflected light does not interfere with the incoming laser, so that half of the emitted light is directed towards the substrate. Having the reflectivity switched to half of this value requires a control laser power of about 3 photons/lifetime, and the reflectivity is mainly coherent.

b. Co-polarized. The reflectivity can reach unity for a vanishing control laser power, and is fully coherent (see Fig.7). This is a key assets for applications in quantum information processing. The switching power required to switch the reflectivity down to a value of 0.5 is 1 photon/lifetime.

[1] Cohen-Tannoudji, C., Dupont-Roc, J., and Grynberg, G., Atom-Photon Interactions, Wiley, New York (1992).

[2] Carmichael, H.J., Statistical Methods in Quantum Optics 1: Master Equations and Fokker-Planck Equations,

Springer, Berlin, Heidelberg (2003).

[3] Auffèves-Garnier, A., Simon, C., Gérard, J.M., Poizat, J.P., Giant Optical Non-linearity induced by a Single Two-Level System interacting with a Cavity in the Purcell Regime, Phys. Rev. A **75**, 053823 (2007)

[4] Valente, D., Portolan, S., Nogues, G., Poizat, J.P., Richard, M., Gérard, J.M., Santos, M.F. and Auffèves, A., Monitoring stimulated emission at the single-photon level in one-dimensional atoms Phys. Rev. A **85**, 023811 (2012).

[5] Nguyen, H.A., Two-mode giant optical non-linearity with a single quantum dot in a photonic waveguide, PhD Thesis, Université Grenoble-Alpes (2016), https://hal.archives-ouvertes.fr/tel-01360549